PathSpace: Rapid continuous map approximation for efficient SLAM using B-Splines in constrained environments

Aduen Benjumea[1], Andrew Bradley[1], Alexander Rast[1], and Matthias Rolf[1]

[1]School of Engineering, Computing & Mathematics, Oxford Brookes University, Oxford, UK

arXiv:2603.02538v1 [cs.RO] 3 Mar 2026

Abstract

Simultaneous Localization and Mapping (SLAM) plays a crucial role in enabling autonomous vehicles to navigate previously unknown environments. Semantic SLAM mostly extends visual SLAM, leveraging the higher density information available to reason about the environment in a more human-like manner. This allows for better decision making by exploiting prior structural knowledge of the environment, usually in the form of labels. Current semantic SLAM techniques still mostly rely on a dense geometric representation of the environment, limiting their ability to apply constraints based on context. We propose PathSpace, a novel semantic SLAM framework that uses continuous B-splines to represent the environment in a compact manner, while also maintaining and reasoning through the continuous probability density functions required for probabilistic reasoning. This system applies the multiple strengths of B-splines in the context of SLAM to interpolate and fit otherwise discrete sparse environments. We test this framework in the context of autonomous racing, where we exploit pre-specified track characteristics to produce significantly reduced representations at comparable levels of accuracy to traditional landmark based methods and demonstrate its potential in limiting the resources used by a system with minimal accuracy loss.

Figure 1: Example of a continuous B-spline representation of using a limited number of control points for its representation. Base map data by OpenStreetMap (available under the Open Database License)

1 INTRODUCTION

Autonomous agents employ Simultaneous Localisation and Mapping (SLAM) as the probabilistic framework to reason through sensor and actuation uncertainty, producing a reliable belief of an agent's state and its environment in previously unknown spaces and aid in later navigation. While specific implementations vary across platforms, from small indoor robots to large autonomous vehicles, they share a core reliance on these principles for navigation. Visual SLAM (VSLAM) often utilizes dense geometric data from visual sensors to optimize relative positions Abaspur Kazerouni et al., 2022. However, these representations frequently fail to capture the contextual information essential for high-level cognition. Semantic SLAM bridges this gap by incorporating object labelling and segmentation directly into the localisation processChen et al., 2022. By moving beyond purely geometric data, the system becomes more robust to granular visual shifts like lighting or perspective changes, allowing the agent to interpret its surroundings conceptually and facilitate more complex, reactively informed tasks.

Semantic SLAM in principle works by leveraging known context about the environment, which has the downside of being more restrictive to a given domain for the benefit of adding valuable contextual information to the system Sualeh and Kim, 2021. Generally speaking, the more tightly structured the domain, the more context can be leveraged as more assumptions of the environment can be made in advance. The idea of anchoring Coradeschi and Saffiotti, 2003 applied to indoor, for example, can relate object detections to label an entire room at a higher abstracted level, usually with the goal of improving human to robot interfaces Galindo et al., 2005. Similar reasoning can be applied to autonomous vehicles, where the known structure of the road can greatly limit the domain of plausible layouts or be used for labelling entire areas of the environment as requiring a higher level of attention Roth et al., 2024. In the context of roads, these can be areas of likely higher traffic, or areas with rapid changes in curvature in the case of high performance scenarios.

B-splines are a staple of geometric representation in CAD design and computer graphics, but despite their extensive representational capabilities including, but not limited to, their smoothing, interpolating and extrapolating capabilities, they are not exploited to their full potential in SLAM systems. The few examples seen as part of a SLAM system often condense rich point cloud data of the environment as several curve objects Pedraza et al., 2009. Their use as the

main representational method of an environment defined by sparse or semantic features or as the main sole object of the environment has, however, barely been looked at. Cubic B-splines possess C2 continuity, guaranteeing a smooth second derivative, which in turn translates to an equivalent smooth acceleration curve and therefore preventing the representation of physically impossible motion paths Gonzalez et al., 2022. Additionally, the local control property of B-splines means an update to a localised area of the curve does not need to affect the entire curve, making it more suitable for live updates given previously seen samples. A representation of a track using a single spline would, by design, reduce the degree of freedom of landmark association and allow for the representation of seamlessly closed circuits. In the world of motorsport, this can lead to maps being represented much closer to how lap time simulation operates, making the map of the system inherently contain semantic information for the task at hand and therefore facilitate integration of optimal paths as a way to allow higher level cognition in the system. Ultimately, such representations can more closely model how a human would understand the environment, and a system with some attention to curvature would inherently allow for embedding maximum speed controls as an example, providing more context for path planning and control sub-systems.

The main contribution of this paper is a novel framework for the use of B-splines to represent continuous distribution of functions in the context of SLAM. We demonstrate how the nature of this representation allows us to drastically limit the redundant complexity of map representations, improving the scalability of such systems and show the feasibility of an online system leveraging this framework within the case study of autonomous racing compared to equivalent traditional methods.

The rest of this paper is organized as follows. In Sec 2 we explore existing work leading up to the current scene in abstract map representations in SLAM. Sec 3 introduces core concepts regarding B-spline manipulations required and their use as a map representation for SLAM systems. Then Sec 4 analyses aspects of our system within the context of a controlled scenario. Finally, in Sec 5 we discuss further challenges open in this field before concluding.

2 RELATED WORK

2.1 SLAM in Autonomous Vehicles

An autonomous vehicle (AV), much like any autonomous mobile robot tasked with navigation, requires four steps to complete its task: perception, localization, cognition and control Siegwart et al., 2011. Localization here is a subtask of SLAM, which leads to the recent interest in advancing these technologies alongside the increased interest in commercial AVs.

A SLAM system can be thought of as offline, where the prediction over the entire history of positions is optimized, or online, where we treat localization as a Markovian process and optimize the current position Thrun and Thrun, 2005. Generally, live systems concerned with autonomy and reactiveness will implement online methods with higher updates rates and greater constraints when it comes to computational resources available.

We can categorize SLAM methods by their mathematical basis. Filter based systems such as the extended Kalman filter (EKF) Thrun, 2002 solve SLAM recursively, processing the state of the vehicle and the map as a prediction or prior and an update based on sensor readings. Variants such as the unscented Kalman filter (UKF)Wan and Van Der Merwe, 2000 provide alternative methods for the linearization of the models involved for increased robustness. Highly non-linear environments frequently opt for a particle filter (PF) approach instead, where smaller state predictions are made over many hypotheses referred to as particles, such as FastSLAM Montemerlo et al., 2003. In optimization based approaches, such as Graph SLAM Grisetti et al., 2011, a front end collects all the system constraints and a backend performs non-linear optimization to obtain a maximum likelihood of states.

2.2 Semantic SLAM

The emergence of high-speed, specialised visual processing in GPUs has resulted in standardised VSLAM approaches, often leveraging bundle adjustmentTriggs et al., 1999 to perform visual odometry Nistér et al., 2004, such as the well known ORB SLAM Mur-Artal et al., 2015. Similar techniques can be applied to other sensors such as LiDAR Shan et al., 2020 or depth cameras Yu et al., 2018.

Furthermore, deep learning has enabled the introduction of object detection and segmentation to these tasks, leading to the field of semantic SLAM extending VSLAM Chen et al., 2022. Providing higher level information into the system decreases the dependence on geometric points, and therefore subtle changes in the sensors domain generally have a lesser impact on the system integrity You et al., 2022. Systems using semantic SLAM range from discrete landmark based systems Bowman et al., 2017, precise object characteristic recognition Pavlakos et al., 2017 or continuous or finely detailed segmentation of the environment Tateno et al., 2017. Semantic SLAM is currently at the frontier of SLAM research Chen et al., 2022, and more complex methods aim at facilitating more complex tasks and increasing autonomy by more closely relating it to the path planning and decision making tasks or allowing for more flexibility in dynamic environments F. Hu et al., 2024.

While VSLAM brings the steps of perception and localization closer together, semantic SLAM can be thought of as bringing the steps of localization and cognition closer together, as it allows for the system to leverage the context of the environment in its localization process, and therefore allows for the system to make more informed decisions based on this context.

2.3 B-splines in SLAM

B-splines are commonly used in product design for their ability to produce continuous surfaces, for light rendering or in animation to produce smooth motion speeds Hasan et al., 2024 and exploit their local control and flexible level of continuity for interpolation with limited parameters. In SLAM however, they are more often used as a means to

represent large and dense cluster of readings consisting of hundreds of points each update cycle as a single condensed object Rodrigues et al., 2021Liu et al., 2009Kanna et al., 2024Pedraza et al., 2007. This reduces the number of redundant points being stored and ultimately reduces unwanted noise by smoothly fitting the data to a simpler surface. When it comes to motion, B-splines have been used in a similar fashion to reduce unwanted prediction noise for the predicted path of an agent Liu et al., 2010, or to interpolate vehicle motion predictions for the purposes of handling asynchronous measurements or issues such as rolling shutter measurements Lovegrove et al., 2013. Another use of B-splines is as surfaces, representing what would otherwise be a discrete occupancy grid map as a continuous surface, which can be leveraged for better predictions in path planning and obstacle avoidance Kanna et al., 2024.

While SLAM research recognises B-splines for their smoothing and compression properties, particularly in representing dense point clusters, their application within semantic frameworks has not been exploited, yet. Specifically, a gap exists in creating more adaptable systems that are able to react to the overall semantic properties of the environment while discerning a continuous probabilistic understanding of the environment solely from discrete features. By utilizing the representational flexibility of B-splines, we can develop a task-oriented probabilistic system that prioritizes environmental features most relevant to the agent, focussing on an alternate representation of the environment that are most suited to organize driving behaviour through path planning and control.

3 B-SPLINE REPRESENTATION

3.1 Fundamentals

A B-spline or basis spline is a piecewise polynomial function $\mathbf{S} = \{k, \mathbf{t}, \mathbf{C}\}$ defined by an integer order k (degree $k-1$), a knot vector $\mathbf{t} = [t_0, t_1, \ldots, t_n]$ and a set of control points (or coefficients) $\mathbf{C} = [c_0, c_1, \ldots, c_n]$ where each C_i has the same dimensionality as the output of the spline. The B-spline at input parameter value u is defined as:

$$S_{\mathbf{t},k}(u) = \sum_{j=0}^{n} C_j \beta_{j,k}(u) \tag{1}$$

Here, $\beta_{j,k}(u)$ are the B-spline basis functions defined by the Cox-de Boor recursionL. Piegl and Tiller, 2012 as follows for $k = 0$ and $k > 0$ respectively:

$$\beta_{j,0}(u) = \begin{cases} 1 & \text{if } t_j \leq u < t_{j+1} \\ 0 & \text{otherwise} \end{cases} \tag{2}$$

$$\beta_{j,k}(u) = \frac{u - t_j}{t_{j+k} - t_j} \beta_{j,k-1}(u) + \frac{t_{j+k+1} - u}{t_{j+k+1} - t_{j+1}} \beta_{j+1,k-1}(u) \tag{3}$$

This can be thought of as a smooth average weighted by β of k control points C_i nearest to u. The knot vector $\mathbf{t}$ effectively tells us the range influence each control point has on the distance from u to the control points, and does not need to be uniform nor requires values to be unique, but it must be non decreasing ($t_i \leq t_{i+1}$). The multiplicity of each value effectively reduces the degree of the spline at that particular point, potentially compromising its continuity. If the multiplicity of values at the ends of the knot vector equals the order k, the spline is said to be clamped (or left/right clamped if asymmetrical)L. A. Piegl et al., 1995, and it guarantees the ends of the spline will interpolate the end control points. We assume a spline will be clamped unless otherwise stated. the processes of clamping or unclamping, then, refer to the increase or decrease of the multiplicity to 0 or the order of the spline of the end knot values respectively. This would often be paired with a recalculation of the control points to preserve the shape of the spline.

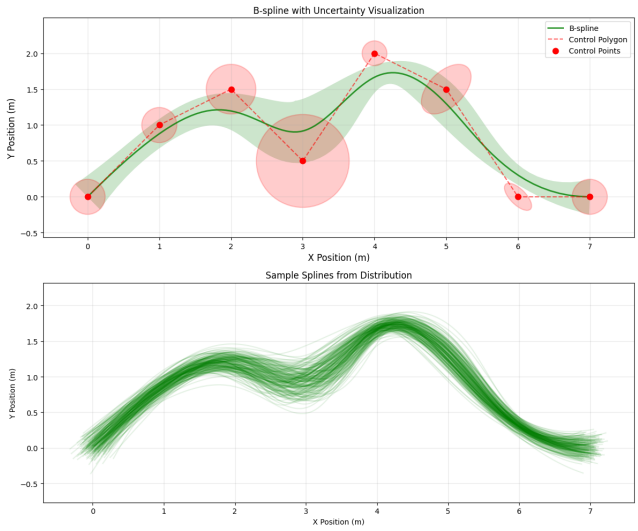

Figure 2: Demonstration of continuous uncertainty representation from discrete control point uncertainties and how it creates a continuous distribution of splines.

3.2 Representing uncertainty

To fully benefit from the the continuous representation B-splines provide for the mean prediction of the environment, we need to represent the uncertainty in an equally continuous manner, allowing any sample along the spline to be associated with a probability distribution.

In line with the rationale of Kalman Filter methods, we represent uncertainty as a single covariance matrix Σ. This matrix tracks the marginal uncertainties of both the agent state and the individual control points, while the off-diagonal cross-covariance terms preserve the dependencies necessary for optimization.

Since each control point provides direct local control of the spline, we associate a Gaussian distribution to each control point, and propagate this uncertainty through the same basis functions that govern the spline itself. Thus, we determine the uncertainty of a point on the spline $\Sigma_{S(u)}$ given the uncertainty of the control points by squaring the basis functions as follows:

$$\Sigma_{S(u)} = \sum_{j=0}^{n} \Sigma_{C_j} (\beta_{j,k}(u))^2 \tag{4}$$

where Σ_{C_j} is the marginalised covariance matrix of the control point C_j within the larger Σ covariance matrix of the

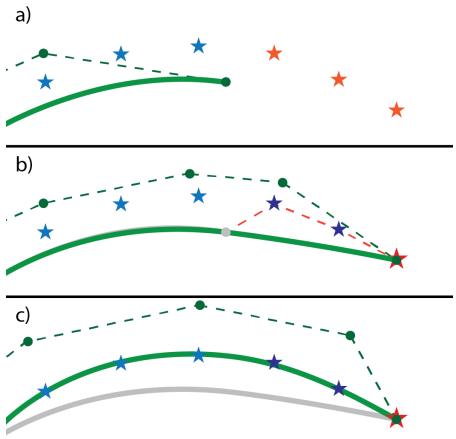

Figure 3: Process of expanding the spline S_z based on new readings $\mathbf{z}$. Each reading $\mathbf{z}_i$ are categorised as expansion points of the closest spline point is $\mathbf{S}(1)$ and is beyond a threshold distance from $\mathbf{C}_n$ and $\mathbf{C}_{n-1}$ or as update points otherwise (a), the interpolation point is selected and the rest are re-categorised while the spline extends to interpolate the new point (b), and an update is performed with all remaining points (c).

entire system, treating the spline as a continuous uncertainty distributions as is illustrated in 2.

3.3 Expansion

Upon the detection of a set of landmarks, the system determines if an extension of the spline is required and where to extend it. Figure 3 illustrates the steps taken to determine and handle an extension of the spline, which begins by determining when a landmark is updating or extending the spline. In order to perform this classification, we employ a function where a measurement point is marked for expansion of the spline when it satisfies a three-part boundary condition: the projection of the landmark onto the spline, i.e. the closest point in the spline must coincide with the terminal parameter $u = 1$, the Euclidean distance to this endpoint must exceed a predefined growth threshold, and the point must maintain sufficient separation from the second-to-last control point C_{n-1} to prevent localized over-parameterization while also avoiding over-stretching of the particular spline segment. It is worth noting that there is a degree of flexibility in parametrizing this heuristic as informed by knowledge and assumptions of the task domain, as well as potential for more complex functions if more constraints can be gleaned from the environment.

Before the update is performed, the points marked for expansion are ordered by a proximity chain with respect to the spline's endpoint. That is, the closest point to $\mathbf{S}(1)$, followed by the closest point to the last in the sequence repeatedly. The last point in this sequence is used to extend the spline, while the rest are re-categorised as update points.

We extend the spline to this point following the methodology described in S.-M. Hu et al., 2002. This process involves unclamping the spline by reducing the multiplicity of the terminal knot value, followed by a recalculation of the local control points to preserve the original shape. The extension point is then inserted as a control point along with uncertainty associated with the sensor reading, and the knot vector $\mathbf{t}$ is re-clamped around it to ensure exact interpolation at the new boundary. Once added, the spline can be updated to fit the remaining points as shown in figure 3

3.4 Update

When one or more landmarks $\mathbf{z}$ are detected and determined to belong to the existing spline, we initially fit a continuous spline with the discrete readings received. Note that for this process, concrete data association is not required, as we are interested in what the landmark is communicating about the environment rather than its specific identity. For this same reason, this transform will combine multiple landmark readings into a singular, continuous spline reading, and thus only a single update will be performed to the relevant control points per perception cycle.

Firstly, we create a copy of the current state spline S_μ. This process will mutate this state to agree with the perceived data. We refer to this newly fit spline as S_z. Figure 4 shows this process. We locate the parameter values u_z along S_μ that would generate the closest point to the reading on the spline, $\bar{\mathbf{z}}$, and note the basis values for each control point used at those u values by our spline as $\mathbf{b}_z$. We use this to populate each row basis matrix$\mathbf{B}$. This matrix is of size mxn where m is the number of readings and n the number of control points.

$$\min_{\mathbf{C}} \|\mathbf{y} - \mathbf{B}\mathbf{C}\|^2 + \|\mathbf{L}(\mathbf{C} - \mathbf{C}_\mu)\|^2 \tag{5}$$

Where $\mathbf{C}_\mu$ is the current position of the control points in the state spline. $\mathbf{L}$ in this case is the regularization parameter, which can often be found expressed as $\mathbf{I}\lambda$ when a uniform regularization is sufficient. In our case however, we require the control points with a higher influence over $\bar{\mathbf{z}}$ to be regularized less, meaning they will have a bias to travel further when fitting. To achieve this , we define it as

$$\mathbf{L} = \lambda \operatorname{diag}\left(\mathbf{1}_n - \frac{1}{m}\mathbf{B}^T\mathbf{1}_m\right)$$

with $\mathbf{1}_m$ and $\mathbf{1}_n$ as column vectors of 1s of the respective size and λ still as a regularization scaling parameter. We then solve for the control points of the fitted spline as

$$\mathbf{C} = (\mathbf{B}^T\mathbf{B} + \mathbf{L})^{-1}(\mathbf{B}^T\mathbf{y} + \mathbf{L}\mathbf{C}_\mu) \tag{6}$$

Note that this method does not guarantee that the readings will be fitted exactly, but rather generates a constrained line of best fit, and has the additional effect of smoothing over contradicting or noisy reading points in benefit of a smooth semantic understanding of the traversable area.

In order to maintain the uncertainty of the reading in this new representation and be able to later use it in the update step of a Kalman filter, we need to be able to propagate the uncertainty of the reading through this fitting process. We do this through the use a Cubature Transfor Arasaratnam and Haykin, 2009, which is a method for propagating uncertainty through non-linear transformations, similar to the Unscented Transform used in the UKF but with a different sampling strategy that can provide better performance in higher dimensions. This process involves the generation

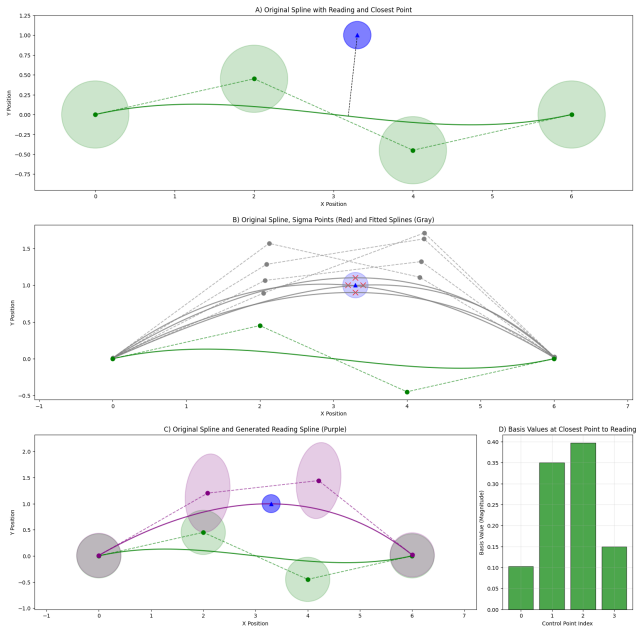

Figure 4: Demonstration of $\mathbf{S}_z$ fitting. In (A) we find the closest point in $\mathbf{S}_\mu$ (green) to a new set of readings $\mathbf{z}$ (blue). In (B) we generate the sigma points $\mathbf{X}$ (red) based on the uncertainty of the reading and fit $\mathbf{S}_\mu$ to each one using ridge regression fitting $h()$ to generate the $\mathbf{Z}$ splines (gray). in (C), the the control points in $\mathbf{Z}$ are averaged to obtain the control points and their respective covariance, defining $\mathbf{S}_z$ (purple). (D) shows the basis values of each control point on the closes spline point to the reading, determining how much each control point will be allowed to move to fit in (B)

of a set of sigma points $\mathbf{X}$ that are representative of the distribution of the reading, which are then passed through $h()$, defined as the aforementioned ridge regression process, to obtain a new set of points in the spline representation $\mathbf{Z}$. The mean and covariance after this transformation can then be calculated as a weighted average of the transformed points, with weights determined by $\mathbf{X}$. More detail on the formulation of these processes can be found in Wan and Van Der Merwe, 2000

From this point, the control point values and their uncertainty can be used directly in the update step of a Kalman filter. Notice how the control point association between the reading and state are direct and do not require additional processing. Traditional discrete methods require some form of matching optimization for landmark association when the landmarks are not uniquely identifiable. This process, by contrast, uses whichever point along the continuous spline is closest to the discrete reading. This means the fitted spline is able to capture how the uncertainty on a landmark interacts with the current direction of the spline, as the sample based transform realises less influential uncertainty directions as shown in fig4. This also directly tackles difficulties with complex data association and avoids duplicate landmarks in the map from misassociation. Additionally, the reading has already been transformed to the representation of the state, so the measurement model for the later filter in the update step is effectively an identity function, simplifying it.

3.5 Simplification

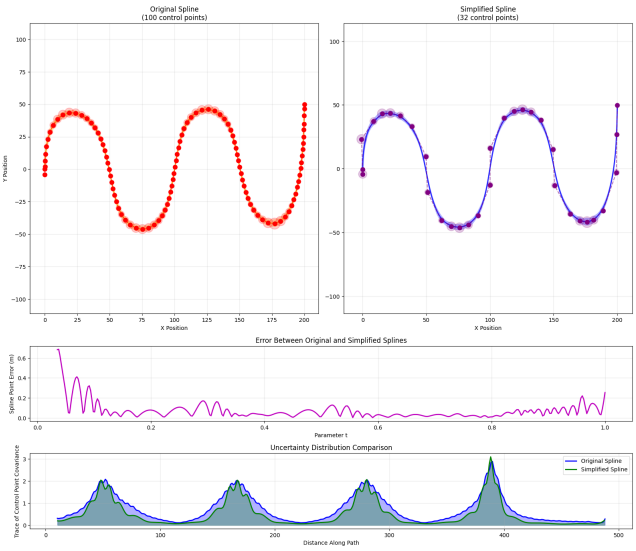

Figure 5: Comparison between sample spline before and after simplification. We show a control point reduction from 100 to 32 points with minimal data loss

To maintain map sparsity and mitigate redundant memory consumption, we employ a curvature weighted simplification that re-allocates representational capacity based on geometric complexity. The process begins by uniformly sampling the existing spline to derive a localized curvature profile, which is then normalized into a probability distribution. A linear baseline is integrated into this distribution to ensure a minimum control point density remains in low-curvature or linear segments, preventing topological gaps. By distributing a target number of knots (determined by the length and complexity of the features of the operational domain) across the resulting cumulative curvature distribution, the algorithm effectively concentrates control points in complex regions such as sharp corners while simplifying redundant data in straight sections. Finally, a new parametric model is generated through a least-squares optimization that fits the reduced set of control points to the original sampled data, ensuring the global shape is preserved while significantly lowering the dimensionality of the map state. Similarly to how we propagate error through our $\mathbf{S}_z$ fitting, we propagate uncertainty of the overparameterized spline through this process using a sample based Cubature Transform, generating sigma points for the state of the spline, performing the simplification once the ideal knot vector has been determined and recollecting the mean and covariance of the simplified spline. This process is performed at a low frequency as it optimizes the entire spline and incurs a considerable computational overhead, but provides a near equivalent representation of the map so far with significantly fewer parameters. Figure 5 compares a spline before and after this operation is performed.

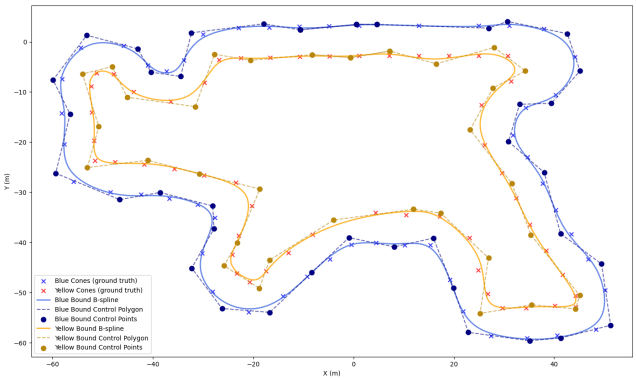

Figure 6: Simulated track setup, showing splines mapping both boundaries over an entire track up to the specification of our case study.

3.6 Experiments

3.6.1 Isolated tests

To validate the core operations of this framework, we experimentally test each of the components described in the previous sections in isolation, using synthetic data to validate the expected behaviour of each of these elements and obtain an initial understanding of useful parameterization and/or possible implementation considerations.

3.6.2 Autonomous Racing

As a proof of concept, we apply this framework to the context of autonomous racing, where the track can be represented as a single closed loop spline as an assumption of the environment. More specifically, we consider its application in the context of Formula Student Driverless, providing a highly controlled environment with composed of circuits demarcated by brightly colored traffic cones, but where the visual features of the track are not guaranteed to be consistent across laps, marked as brightly colored cones. In collaboration with the Oxford Brookes Racing Autonomous Team, we build on top of a pre-existing front end, providing 3D cone detections semantically with their respective label and uncertainty measure. The goal in this scenario is to map the differently coloured cone boundaries (blue and yellow), demonstrating feasibility, stability and resource usage of this methodology when applied to a real-world application requiring the use of a computationally-efficient SLAM approach.

4 Results

4.1 Simulation setup

Following the case study of autonomous racing, we generate a synthetic track with similar characteristics to those found in the real application based on technical specification of the competition and reconstructions from aerial images taken in real world testing. This includes the separation between landmarks (cones), track boundaries and overall track length, as well as the expected track elements such as straights, hairpins and chicanes. For the purpose of testing the core functionality of the system, we isolate the backend by assuming a known front end, providing cone detections with their associated uncertainty as well as providing odometry data for the agent. We then allow the agent to run several laps around the track, noting the scale and accuracy of the map generated. Figure 6 shows this layout.

Table 1: Comparison of PathSpace B-spline system against baseline point-based CKF method across multiple track laps of a track with 200 landmarks.

Lap	PathSpace		CKF	
	RMSE (m)	Size	RMSE (m)	Size
1	0.680	133	0.489	156
2	0.658	79	0.487	165
3	0.599	79	0.490	166
4	0.615	79	0.490	167
5	0.600	79	0.491	169

As a baseline, we compare our B-spline system against a traditional landmark-based representation of the track, implementing a CKF with a similarly structured state and overall implementation style. Since landmarks in this case study are not uniquely identifiable, we perform data association in this baseline using the Hungarian algorithm. This solves a set matching optimization given a cost matrix. In this case, we provide this cost as the Mahalanobis distance between mapped landmarks and perceived landmarks to account for evolving landmark certainty and more accurately model landmark association as it would be implemented in a live system.

4.2 Simulation results

We note the absolute error and map size of both methods across several laps of the track in terms of number of control points in the case of PathSpace or landmarks in the case of CKF. Once the system detects the spline exceeding a threshold length and detecting association with early segments of it, the PathSpace system detects the completion of the first lap, closes the spline into a loop and performs a simplification cycle. From this point, no new landmarks are added to the system. Table 1 shows the results of this comparison. We report the result of both boundaries combined in the case of PathSpace. In both cases, we report the RMSE error between the ground truth and the mapped points for CKF or closest spline point for PathSpace at the end of each lap.

We note how the map size in the case of PathSpace is much more consistent and only a fraction of the real number of landmarks in the map (200). In the case of CKF in comparison there is a chance landmarks are duplicated due to misassociations (at times referred to as ghosting) or to discover previously unseen landmarks as new observations due to slight variations in odometry. Since CKF is also unable to map every landmark due to blind spots in the motion of the vehicle, the map will be incomplete. PathSpace in contrast inherently interpolates between these blind spots and still be able to close the circuit and estimate beyond range of sight.

PathSpace does however show slightly lower accuracy than our baseline comparison, but consider the level accuracy adequate for the use case presented, as supported by Brayshaw and Harrison, 2005 showing race lines taken by

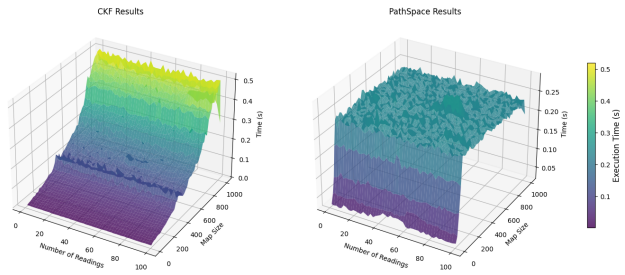

Figure 7: Scalability comparison of a traditional CKF implementation (top) against our B-spline representation (bottom) in terms of both number of landmarks in the map and number of landmarks observed per update. each point represents the average execution time of 10 update cycles.

professional racing drivers to vary by more than $\pm 1m$.

4.3 Scalability

We further investigate the scalability of our B-spline system against a traditional point-based CKF implementation in terms of both the number of landmarks in the map and the number of landmarks observed per update. We compare the execution time for an update cycle in similar conditions for a wide range of parameter combinations. Figure 7 shows the results of this comparison. These results demonstrate that while PathSpace has a higher initial cost due to the fitting and transformation into the spline representation, this same representation limits the computational cost of the update step as the number of landmarks increases based on the expansion and simplification processes, while the point-based method scales cubically. This is due to PathSpace's ability to simplify the map and interpolate between landmarks. This essentially sets a maximum complexity budget for the system, and therefore the execution flattens when the system finds an optimal representation for the given layout. It is worth noting that the specific complexity at which PathSpace plateaus will depend on the parameterization of the system and can therefore be optimised further for a specific system. The number of readings per update did not show a significant effect on the computational cost of either method when compared to map size. Larger reading sizes were not considered as they are unlikely in real world applications.

5 Discussion

PathSpace establishes the first method in literature to extract spline based probabilistic maps online and directly from noisy sensor data. The immediate strength lies in its ability to create a representational budget to optimize the required map size to the complexity of the environment. B-splines do however possess other properties that can further benefit an autonomous agent and can be the basis of a wide range of sub-systems that can make use of such innate representations to further benefit in terms of efficiency. While we have focussed on demonstrating the general feasibility and correctness of this approach, however there is significant potential to encode more complex representations, such as using the spline as a path with a width rather than representing both bounds or otherwise detecting some other property of interest that would not usually be captured from landmark detections, such as conditions or risk of the traversable area. The work presented here demonstrates the feasibility of this type of representation, and opens research in ways to further optimize and exploit this approach to mapping, trading accuracy for more compact representation, with great potential in providing further semantic information to the system.

6 Conclusion

In this paper, we introduce PathSpace, a novel framework to represent probabilistic structured environments in a continuous manner using B-splines in the context of SLAM with a focus on scalability and compactness. We achieve a comparable performance to equivalent traditional methods while reducing the required state size by 53% with systems to optimize the map under this representation. We how PathSpace uses this system to limit the computational resources used while traditional methods scale indefinitely with perceived landmarks and discuss the potential of this type of representation in bringing autonomous systems to a more intuitive and task-oriented level. Future research directions can further leverage the results of this paper by building on top of live systems and and exploit the inherit semantic elements of this methodology to develop smarter and efficient control systems.

We demonstrate a potential implementation and benefits of such a system in the context of autonomous racing, showing how it can leverage the known structure of the track to generate a compact representation of the environment while retaining competitive accuracy.

The potential reduction in computational cost offered by PathSpace's efficient representations paves the way for a new breed of SLAM algorithms based upon encoding critical and semantic environmental features. This would enable more scalable systems able to operate in larger areas seamlessly while offloading post-processing on other subsystems, allowing for more efficient systems both computationally and performance-wise.

References

Abaspur Kazerouni, I., Fitzgerald, L., Dooly, G., & Toal, D. (2022). A survey of state-of-the-art on visual slam. *Expert Systems with Applications*, *205*, 117734. https://doi.org/https://doi.org/10.1016/j.eswa.2022.117734

Arasaratnam, I., & Haykin, S. (2009). Cubature kalman filters. *IEEE Transactions on Automatic Control*, *54*(6), 1254–1269. https://doi.org/10.1109/TAC.2009.2019800

Bowman, S. L., Atanasov, N., Daniilidis, K., & Pappas, G. J. (2017). Probabilistic data association for semantic slam. *2017 IEEE international conference on robotics and automation (ICRA)*, 1722–1729.

Brayshaw, D., & Harrison, M. (2005). A quasi steady state approach to race car lap simulation in order to understand the effects of racing line and centre of gravity location. *Proceedings of the Institution of Mechanical Engineers, Part D: Journal of Automobile Engineering*, *219*(6), 725–739.

Chen, W., Shang, G., Ji, A., Zhou, C., Wang, X., Xu, C., Li, Z., & Hu, K. (2022). An overview on visual slam: From tradition to semantic. *Remote Sensing*, *14*(13). https://doi.org/10.3390/rs14133010

Coradeschi, S., & Saffiotti, A. (2003). An introduction to the anchoring problem. *Robotics and autonomous systems*, *43*(2-3), 85–96.

Galindo, C., Saffiotti, A., Coradeschi, S., Buschka, P., Fernandez-Madrigal, J.-A., & González, J. (2005). Multi-hierarchical semantic maps for mobile robotics. *2005 IEEE/RSJ international conference on intelligent robots and systems*, 2278–2283.

Gonzalez, M., Marchand, E., Kacete, A., & Royan, J. (2022). Twistslam: Constrained slam in dynamic environment. *IEEE Robotics and Automation Letters*, *7*(3), 6846–6853. https://doi.org/10.1109/LRA.2022.3178150

Grisetti, G., Kümmerle, R., Stachniss, C., & Burgard, W. (2011). A tutorial on graph-based slam. *IEEE Intelligent Transportation Systems Magazine*, *2*(4), 31–43.

Hasan, M. S., Alam, M. N., Fayz-Al-Asad, M., Muhammad, N., & Tunç, C. (2024). B-spline curve theory: An overview and applications in real life. *Nonlinear Engineering*, *13*(1), 20240054.

Hu, F., Zong, Q., Mou, X., Chen, Y., Wang, H., & He, M. (2024). A semantic slam system for dynamic environments. *International Conference on Automation and Intelligent Technology (ICAIT 2024)*, *13401*, 165–173.

Hu, S.-M., Tai, C.-L., & Zhang, S.-H. (2002). An extension algorithm for b-splines by curve unclamping. *Computer-Aided Design*, *34*(5), 415–419.

Kanna, B. R., Av, S., Hemalatha, C. S., & Rajagopal, M. K. (2024). Enhancing slam efficiency: A comparative analysis of b-spline surface mapping and grid-based approaches. *Applied intelligence (Boston)*. https://doi.org/10.1007/s10489-024-05776-5

Liu, M., Liu, M., Huang, S., Huang, S., Dissanayake, G., & Dissanayake, G. (2009). A new observation model for b-spline slam. *null*. https://doi.org/null

Liu, M., Liu, M., Huang, S., Huang, S., Dissanayake, G., Dissanayake, G., Kodagoda, S., & Kodagoda, S. (2010). Towards a consistent slam algorithm using b-splines to represent environments. *null*. https://doi.org/10.1109/iros.2010.5649703

Lovegrove, S., Patron-Perez, A., & Sibley, G. (2013). Spline fusion: A continuous-time representation for visual-inertial fusion with application to rolling shutter cameras. *BMVC*, *2*(5), 8.

Montemerlo, M., Thrun, S., Koller, D., Wegbreit, B., et al. (2003). Fastslam 2.0: An improved particle filtering algorithm for simultaneous localization and mapping that provably converges. *IJCAI*, *3*(2003), 1151–1156.

Mur-Artal, R., Montiel, J. M. M., & Tardos, J. D. (2015). Orb-slam: A versatile and accurate monocular slam system. *IEEE transactions on robotics*, *31*(5), 1147–1163.

Nistér, D., Naroditsky, O., & Bergen, J. (2004). Visual odometry. *Proceedings of the 2004 IEEE Computer Society Conference on Computer Vision and Pattern Recognition, 2004. CVPR 2004.*, *1*, I–I.

Pavlakos, G., Zhou, X., Chan, A., Derpanis, K. G., & Daniilidis, K. (2017). 6-dof object pose from semantic keypoints. *2017 IEEE international conference on robotics and automation (ICRA)*, 2011–2018.

Pedraza, L., Pedraza, L., Dissanayake, G., Dissanayake, G., Miró, J. V., Miro, J. V., Rodríguez-Losada, D., Rodriguez-Losada, D., Matía, F., & Matía, F. (2007). Bs-slam: Shaping the world. *null*. https://doi.org/10.15607/rss.2007.iii.022

Pedraza, L., Pedraza, L., Pedraza, L., Rodríguez-Losada, D., Rodriguez-Losada, D., Matía, F., Matía, F., Dissanayake, G., Dissanayake, G., Miró, J. V., & Miro, J. V. (2009). Extending the limits of feature-based slam with b-splines. *IEEE Transactions on Robotics*. https://doi.org/10.1109/tro.2009.2013496

Piegl, L., & Tiller, W. (2012). *The nurbs book*. Springer Science & Business Media.

Piegl, L. A., Piegl, L. A., Tiller, W., & Tiller, W. (1995). The nurbs book. *null*. https://doi.org/null

Rodrigues, R. T., Rodrigues, R. T., Tsiogkas, N., Tsiogkas, N., Pascoal, A., Pascoal, A. M., Aguiar, A. P., & Aguiar, A. P. (2021). Online range-based slam using b-spline surfaces. *IEEE Robotics and Automation Letters*. https://doi.org/10.1109/lra.2021.3060672

Roth, P., Nubert, J., Yang, F., Mittal, M., & Hutter, M. (2024). Viplanner: Visual semantic imperative learning for local navigation. *2024 IEEE International Conference on Robotics and Automation (ICRA)*, 5243–5249.

Shan, T., Englot, B., Meyers, D., Wang, W., Ratti, C., & Rus, D. (2020). Lio-sam: Tightly-coupled lidar inertial odometry via smoothing and mapping. *2020 IEEE/RSJ international conference on intelligent robots and systems (IROS)*, 5135–5142.

Siegwart, R., Nourbakhsh, I. R., & Scaramuzza, D. (2011). *Introduction to autonomous mobile robots*. MIT press.

Sualeh, M., & Kim, G.-W. (2021). Semantics aware dynamic slam based on 3d modt. *Sensors*, *21*(19). https://doi.org/10.3390/s21196355

Tateno, K., Tombari, F., Laina, I., & Navab, N. (2017). Cnn-slam: Real-time dense monocular slam with learned depth prediction. *Proceedings of the IEEE Conference on Computer Vision and Pattern Recognition (CVPR)*.

Thrun, S. (2002). Probabilistic robotics. *Communications of the ACM*, *45*(3), 52–57.

Thrun, S., & Thrun, S. (2005). Probabilistic robotics. *null*. https://doi.org/null

Triggs, B., McLauchlan, P. F., Hartley, R. I., & Fitzgibbon, A. W. (1999). Bundle adjustment—a mod-

ern synthesis. *International workshop on vision algorithms*, 298–372.

Wan, E. A., & Van Der Merwe, R. (2000). The unscented kalman filter for nonlinear estimation. *Proceedings of the IEEE 2000 adaptive systems for signal processing, communications, and control symposium (Cat. No. 00EX373)*, 153–158.

You, Y., Wei, P., Cai, J., Huang, W., Kang, R., & Liu, H. (2022). Misd-slam: Multimodal semantic slam for dynamic environments. *Wireless Communications and Mobile Computing*, *2022*(1), 7600669.

Yu, C., Liu, Z., Liu, X.-J., Xie, F., Yang, Y., Wei, Q., & Fei, Q. (2018). Ds-slam: A semantic visual slam towards dynamic environments. *2018 IEEE/RSJ international conference on intelligent robots and systems (IROS)*, 1168–1174.